Journal of Catalysis **210,** 7–16 (2002)
doi:10.1006/jcat.2002.3612

Hydrogen Production Using Ni–Rh on La_2O_3 as Potential Low-Temperature Catalysts for Membrane Reactors

S. Irusta, L. M. Cornaglia, and E. A. Lombardo[1]

Instituto de Investigaciones en Catálisis y Petroquímica (FIQ, UNL-CONICET), Santiago del Estero 2829, 3000 Santa Fe Argentina

Received August 27, 2001; revised February 19, 2002; accepted February 19, 2002

The activity and stability of Ni–Rh mono and bimetallic catalysts supported on lanthanum oxide was studied. The catalysts were prepared by wet impregnation with different contents of Rh and 2 wt% Ni. The solids were calcined at 823 K in air flow and were reduced at 973 K in flowing hydrogen. The results of the catalytic evaluation in a fixed-bed reactor showed that the Rh solids had the highest activity at 823 K. In order to understand the Rh effect, the catalysts were characterized through XRD, XPS, and TPR. No evidence of crystalline Ni phase through XRD was observed in either the calcined or used catalysts. On the other hand, the TPR results suggested a significant metal–support interaction. The XPS data is consistent with this picture. Bimetallic catalysts presented the highest amount of carbon deposits. TGA, DSC, and SEM were used in order to characterize the carbonaceous species. On the catalyst surface at least two types of carbons were detected with different structural properties which did not deactivate the solid. A low carbon deposition was observed on Rh (0.2%)/La_2O_3 which exhibited a stable activity after 100 h on stream.

Key Words: **hydrogen; CO_2 reforming; Ni–Rh catalysts.**

INTRODUCTION

Hydrogen is a potentially nonpolluting, inexhaustible, efficient, highly cost-attractive fuel. The production of hydrogen through the methane-reforming reaction with carbon dioxide employing a membrane reactor seems to be an interesting approach since it also combines two gases that produce the greenhouse effect (1). An active, long-life catalyst at low temperature (<870 K) is a key player in this system.

The carbon dioxide reforming of methane to obtain hydrogen and carbon monoxide has recently captured the attention of many researchers. Due to their low cost, Ni-based catalysts are often preferred (2–4). Most catalysts reported in the literature can reach the equilibrium conversions by adequately adjusting the contact time. However, this reaction is accompanied by the undesired formation of different kinds of carbon deposits. In these systems, the deactivation can be fast and the catalysts can become inactive after a short reaction time (5).

There is general agreement in the literature about the good properties of noble-metal-based catalysts (6–9). They show a better activity and less carbon deposition than non-noble-metal systems. Numerous studies have been carried out to develop an effective catalyst and learn more about the reaction and deactivation mechanism. Rhodium has been supported on different oxides. Metal–support interaction, dispersion, and particle size have been proposed as the main factors which defined the solid ability to catalyze both the desired reaction and the carbon deposition.

The dry-reforming methane reaction carried out in a fixed-bed reactor is limited by the equilibrium conversions. Since this reaction is highly endothermic, it is favored at temperatures higher than 973 K. The use of a membrane reactor to extract one of the reaction products allows not only an overcoming of the thermodynamic limitation but also a shift in the working range to lower temperatures, with the subsequent energy-saving effects (10).

The objective of the present work is to study the activity and stability of Ni–Rh mono- and bimetallic catalysts supported on lanthanum oxide in the CO_2 reforming of methane at low temperature; these catalysts are to be used in a membrane reactor. The catalysts were characterized by XRD, XPS, and temperature-programmed reduction while the carbon deposit was studied through thermal analysis (TGA and DSC), SEM, and laser Raman spectroscopy.

EXPERIMENTAL

Catalyst Preparation

Catalysts were prepared by conventional wet impregnation of La_2O_3 (Anedra, 99.99%) using $Ni(NO_3)_2 \cdot 6H_2O$ and $RhCl_3 \cdot 3H_2O$ as precursor compounds. The bimetallic solid was prepared by simultaneous impregnation. In all cases, the resulting suspension was then heated at 353 K to evaporate the water and the solid material was dried in an oven at 383 K overnight. The resulting catalysts were calcined for 6 h at 823 K with a heating rate of 1.8 K/min.

[1] To whom correspondence should be addressed. E-mail: nfisico@fiqus.unl.edu.ar.

0021-9517/02 $35.00

Catalyst Testing

The catalyst was loaded into a tubular quartz reactor (i.d., 5 mm) which was placed in an electric oven. A thermocouple in a quartz sleeve was positioned on top of the catalyst bed. The reaction products were analyzed with a TCD gas chromatograph (Shimadzu GC-8A) equipped with a Porapak and a molecular sieve column. The catalysts were heated in He at 973 K and then reduced *in situ* in H_2 at the same temperature for 0.5 h. After reduction, the reaction temperature was reached in flowing He and the feed gas mixture (33% (v/v) CH_4, 33% CO_2, 34% He, $P = 1$ atm) was then switched to the reactor. Three different types of catalytic measurements were carried out: (i) with 300 mg of catalyst, at $W/F = 1.07 \times 10^{-5}$ g h ml^{-1} at 823, 873, 923, and 973 K, with total time on stream 48 h (W, mass of catalyst; F, total gas flow rate); (ii) with reaction rates obtained at 823 K, with the reactor operating in differential mode using 50 mg of catalyst; and (iii) with stability tests carried out at 823 K, with 50 mg of solid at $W/F = 2.67 \times 10^{-5}$ g h ml^{-1} and conversion measured at $W/F = 4.50 \times 10^{-6}$ g h ml^{-1}.

Surface Area and X-Ray Diffraction (XRD)

For the determination of the surface area of calcined and used solids, a Quantachrome Sorptometer, Nova 1000 model, was employed. Prior to the BET measurements the samples were maintained at 473 K under vacuum of 10^{-3} Torr for 2 h.

The XRD patterns of the calcined and used solids were obtained with an XD-D1 Shimadzu instrument, using Cu $K\alpha$ radiation at 35 kV and 40 mA. The scan rate was 1°/min for values between $2\theta = 10$ and 80°.

Metal Dispersion

The Rh dispersion of fresh catalysts, following the H_2 reduction at 973 K for 0.5 h, was determined by static equilibrium H_2 adsorption at room temperature in a conventional vacuum system. As a standard procedure, prior to adsorption, the catalysts (300 mg) were evacuated (10^{-5} Torr) at 773 K (Rh (0.2%) and Rh (0.6%)) or 973 K (Ni(2%)) for 1 h. In order to determine the evacuation temperature, H_2 desorption experiments were carried out using a flow reactor. This procedure was as follows: after reduction at 973 K for 0.5 h, the catalyst was rapidly cooled to 573 K in He, exposed to H_2 flow for 1 h, and then cooled to 300 K and maintained for 30 min under H_2 flow. The feed was switched to He and the desorbing H_2 was measured with an online Balzers Quadstar TU 422 mass spectrometer.

Temperature-Programmed Reduction (TPR)

An Ohkura TP-20022S instrument equipped with TCD was used for the TPR experiments. To eliminate the carbonates present in the samples, two different treatments were carried out before the TPR tests. (A) The samples (100 mg) were heated to 1123 K in flowing oxygen. The temperature was kept constant for half an hour; then, the samples were cooled in an Ar stream. (B) The samples were heated to 823 K in oxygen flow. This temperature was kept constant for 2 h; then, the samples were cooled in an Ar flow. Afterward, they were reduced in a 5% H_2–Ar stream, with a heating rate of 10 K/min up to the maximum treatment temperature .

X-Ray Photoelectron Spectroscopy

The XPS measurements were carried out using an ESCA750 Shimadzu electron spectrometer. Nonmonochromatic Al $K\alpha$ X-ray radiation was used. The anode was operated at 8 kV and 30 mA and the pressure in the analysis chamber was about 2×10^{-6} Pa.

The binding energies (BE) were referred to the C 1s signal (284.6 eV). Curve fitting was performed using a Levenberg–Marquardt NLLSCF routine. The background contribution was taken into account by assuming an integral-type background. The surface Rh/La and Ni/La atomic ratios were calculated using the areas under the Rh 3d, Ni $2p_{1/2}$, and La $3d_{5/2}$ peaks, the Scotfield photoionization cross sections, the mean free paths of the electrons, and the instrumental function, which was given by the ESCA manufacturer.

Thermogravimetric Analysis

The amount of carbon on the used catalysts was determined by oxidizing the carbon in a Mettler Toledo TGA/SDTA 851. The used catalysts (usually 10 mg) were heated at 10 K min^{-1} to 1173 K in a flow of 90 ml min^{-1} air.

Thermal analysis experiments were carried out in a Mettler Toledo DSC 821^e in order to find out the exothermic or endothermic nature of the changes that take place during the calcination of the used solids.

Scannig Electron Microscopy (SEM)

The morphology of the carbon deposits was studied using a JEOL microscope, Model JSM-35C, operated at accelerating voltages of 20–25 kV. The used solids were glued to the sample holder with silver paint and covered with a thin gold layer to improve the images.

Laser Raman Spectroscopy (LRS)

The Raman spectra were recorded with a TRS-600-SZ-P Jasco Laser Raman instrument, equipped with a CCD (charge-coupled device) with the detector cooled to about 153 K using liquid N_2. The excitation source was the 514.5-nm line of a Spectra 9000 Photometrics Ar ion laser. The laser power was set at 30 mW.

RESULTS

Catalytic Behavior, Stability, and TOFs

The catalytic activity was measured at a given space velocity and different temperatures (823–973 K) for a period of 48 h. Conversions at 973 K are shown in Table 1. CH_4 and CO_2 conversions were high and approached equilibrium over all the temperature range. In consequence, higher space velocities were required to operate the reactor in differential mode to calculate the reaction rates. As an example, Fig. 1 shows the methane and carbon dioxide conversions of the bimetallic solid vs residence time. The reaction rates obtained at 823 K for all the catalysts are reported in Table 1. Note that the increase of the Rh content from 0.1 to 0.2% results in a significant increase in the reaction rates for CH_4 and CO_2 disappearance. But a further increase to 0.6% Rh only slightly improves the performance.

The hydrogen TPD profile (not shown) over Rh (0.6%) catalysts exhibits one peak starting at 673 K, with the maximum at 773 K. In the Rh (0.2%) profile, two H_2 peaks are recorded, at 673 and 773 K. In the Ni catalyst, one peak appears, at 1070 K. No hydrogen desorption was observed for the Ni (2%)–Rh (0.2%) catalyst up to 1073 K.

The determination of metal dispersion in monometallic Rh catalysts was performed after evacuation at 773 K for 1 h to complete H_2 desorption after reduction. The Ni-containing catalysts were evacuated at 1023 K (Table 1). The H/metal ratios obtained are shown in Table 1. There is good agreement between this ratio obtained through TPD experiments and the one measured by hydrogen chemisorption.

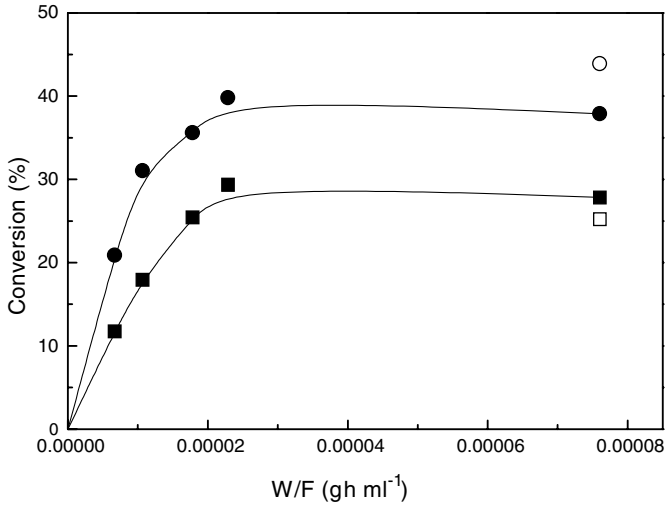

FIG. 1. Catalytic behavior of Ni (2%)–Rh (0.2%) solid at 823 K, 33% (v/v) CH_4, 33% CO_2, 34% He, $P = 1$ atm. ■, CH_4 conversion; ●, CO_2 conversion. Open symbols are for equilibrium values considering the WGS reaction.

With this dispersion, the TOF (Table 2) was calculated as proposed by Mark and Maier (11).

Conversion values were used to evaluate catalyst stabilities. As is clearly shown in Fig. 2, over a testing period of 100 h at 823 K there is practically no loss of activity of the catalysts assayed.

The BET surface area of the fresh catalysts are the same as the support and the same happens with used Rh

TABLE 1

Catalytic Performance and TPR Data of Ni–Rh/La_2O_3 Solids

Catalyst[a]	X_{CH_4}[b] (%)	X_{CO_2}[b] (%)	R_{CH_4}[c] (mol h^{-1} g^{-1})	R_{CO_2}[c] (mol h^{-1} g^{-1})	H/M[d] (mol h^{-1} g^{-1})	TPR data			
						H_2/M[e,f]	T_{Max}[e] (K)	H_2/M[g,f]	T_{Max}[g] (K)
Rh (0.1%)	—	—	0.07	0.19	—	—	—	—	—
Rh (0.2%)[h]	74.8	87.3	0.20	0.42	0.64	0.82	433	0.88	481
	(76.6)	(84.9)			(773 K)[i]		490		545
Ni (2%)	78.5	84.0	0.12	0.21	0.06	0.58	590	0.33	618
					(1023 K)[i]			0.56	765
Ni (2%)–Rh (0.2%)	75.0	87.1	0.24	0.42	0	0.60	559	0.31	586
					(1023 K)[i]			0.60	813
Rh (0.6%)	81.6	90.6	0.26	0.51	0.14	—	—	0.49	482
					(773 K)[i]				546

[a] Solids were reduced *in situ* at 973 K before reaction. Weight percent of the transition metals is in parentheses.

[b] Conversions measured at: reaction temperature, 973 K; $W/F = 1.05 \times 10^{-5}$ g h ml^{-1}; total reaction time, 48 h. Equilibrium values considering the WGS reaction is in parentheses.

[c] Reaction rates measured at 823 K.

[d] Obtained by H_2 chemisorption. M = Ni or Rh.

[e] Treatment temperature, 823 K.

[f] Ratio of micromoles of H_2 to micromoles of metal. M = Rh, Ni or Ni + Rh.

[g] Treatment temperature, 1123 K.

[h] The catalytic activity did not change when the reduction temperature was 823 K.

[i] Evacuation temperature after reduction.

TABLE 2

Reaction Rates, TOF Values, and Deactivation of Ni and Rh Catalysts

Catalyst	D (%)	Temp. (K)	R_{CH_4}[a] mol $h^{-1}g^{-1}$	R_{CH_4}[a] mol $h^{-1}g$ Rh^{-1}	R_{CO_2}[a] mol $h^{-1}g^{-1}$	R_{CO_2}[a] mol $h^{-1}g$ Rh^{-1}	TOF (s^{-1}) CH_4	TOF (s^{-1}) CO_2	θ_{react}[b] (h)	Deac[c] (%)	Ref.
Rh (0.2%)/La_2O_3	64[d]	823	0.20	100	0.42	210	4.4	9.1	100	0	This work
Rh (0.6%)/La_2O_3	14[d]	823	0.26	43	0.51	85	13.8	16.7	100	0	This work
Rh (0.5%)/ZrO_2	90[d]	875	—	—	0.34	68	—	2.2	70	0	6
Rh (0.5%)/Al_2O_3	68[d]	875	—	—	0.55	110	—	4.6	70	0	6
Rh (0.5%)/SiO_2[e]	48[d]	875	—	—	0.10	20	—	1.2	70	70	6
Rh (1.0%)/Al_2O_3	28[f]	873	0.11	11	—	—	1.1	—	48	0	11
Rh (1.0%)/ZrO_2	16[f]	873	0.05	5	—	—	0.9	—	48	0	11
Rh (1.0%)/SiO_2	8[f]	873	0.03	3	—	—	1.2	—	48	0	11
Rh (1.0%)/TiO_2	17[f]	873	0.07	7	—	—	1.3	—	48	0	11
Rh (0.5%)/La_2O_3[e]	20[f]	923	0.21	42	—	—	6.0	—	8	30	21
Rh (3.8%)/SiO_2[e]	11[f]	823	0.06	1.6	—	—	0.36[g]	—	32	—	9
Rh (3.3%)/VO_x/SiO_2[e]	6[f]	823	0.97	14	—	—	6.7[g]	—	32	—	9
Ni (2.0%)/La_2O_3	6[d]	823	0.12	6	0.21	10	1.7	2.5	100	0	This work
Ni (2.0%)/SiO_2	14[d]	873	—	—	0.27	13	—	1.5	—	—[h]	23

[a] Reaction rates calculated from data given by the authors.
[b] Time on stream.
[c] Deactivation.
[d] Dispersion measured by H_2 chemisorption.
[e] Initial value.
[f] Dispersion measured by CO chemisorption.
[g] Calculated using $r = k \cdot p_{CH_4}^{0.22} \cdot p_{CO_2}^{0.23}$ by the authors.
[h] Average deactivation rate, 2.8% h^{-1}.

monometallic solids (Table 3). But after 48 h on stream the surface area of the Ni (2%) doubles while that of the bimetallic solid is seven times higher.

The XRD patterns (not shown) of calcined Rh catalysts show the fingerprints of $La_2O_2CO_3$, La_2O_3, and $La(OH)_3$.

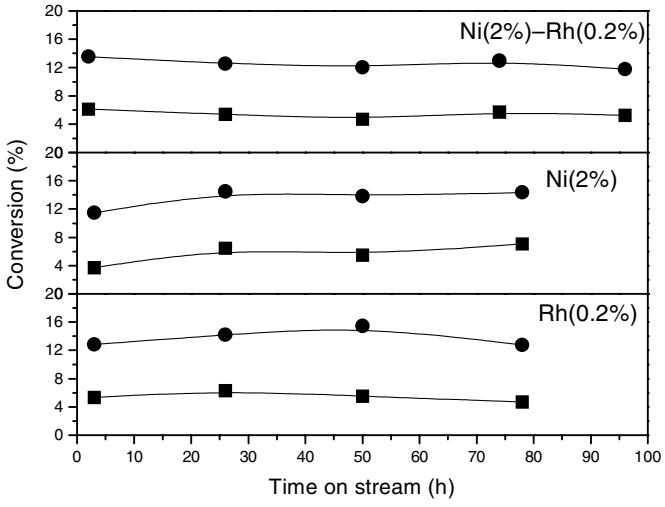

FIG. 2. Stability test. Methane (■) and carbon dioxide (●) conversion over $La_2O_3^-$ supported catalysts. Reaction temperature, 823 K; 33% (v/v) CH_4; 33% CO_2; 34% He; $P = 1$ atm; $W/F = 4.50 \times 10^{-6}$ g h ml^{-1} for Rh (0.2%) and Ni (2%)–Rh (0.2%), $W/F = 1.07 \times 10^{-5}$ g h ml^{-1} for Ni (2%).

In the used solids the hydroxide disappears. In the Ni-containing catalysts, calcined and used, only oxycarbonates and lanthanum oxide peaks were observed.

TPR Data

The hydrogen consumption of the fresh catalysts was calculated from the TPR experiments (Table 1). The TPR profiles of all solids show two peaks after the high-temperature treatment (Fig. 3). The profiles for monometallic Ni and Rh supported on silica were measured for comparison.

The Ni/SiO_2 profile presents only one peak, at 629 K, indicating that there is no significant metal–support interaction. The NiO TPR profile shows a single peak, at 693 K (12), while the Ni (2%) reduction profile reveals two peaks, at 618 and 760 K. The low-temperature peak may be assigned to well-dispersed nickel oxide in the support while the high-temperature peak suggests that the reducibility of some of the nickel ions decreased by strong interactions with the support, possibly by formation of a nickel spinel or perovskite. However, no crystalline phases containing Ni or Rh were observed on any of the samples using XRD.

The Rh catalysts show two peaks, at 481 and 545 K (Table 1), independently of the Rh loading. The Rh/SiO_2 system also exhibits a single reduction peak, at 395 K. The appearance of the highest temperature TPR peak in the Rh/La_2O_3 catalysts as compared to the SiO_2 solid indicates that there is a significant interaction between rhodium oxide

TABLE 3

Surface Area and TGA Data of Ni–Rh/La_2O_3 Solids

Catalyst	S (m^2 g^{-1})		TGA (mg g_{cat}^{-1})					
			$\theta_{react} = 48$ h[a]			$\theta_{react} = 100$ h[b]		
	Fresh	$\theta_{react} = 48$ h[a]	640 K[c]	900 K	1100 K	640 K[c]	900 K	1100 K
Rh (0.2%)	7.6	7.3	0	0	120	61	0	33
Ni (2%)	7.6	16.3	0	0	120	0	147	64
Ni (2%)–Rh (0.2%)	7.4	51.8	0	394	55	0	332	54
Rh (0.6%)	7.3	10.0	11	0	82	—	—	—

[a] Time on stream (reaction temperature, 823–973 K; $W/F = 1.07 \times 10^{-5}$ g h ml^{-1}).
[b] Reaction temperature, 823 K; $W/F = 2.67 \times 10^{-5}$ g h ml^{-1}.
[c] Assigned to water desorption according to DSC data in Fig. 6.

and the La_2O_3 support. The same effect was reported by Wang and Ruckeinstein (13). They reported the presence of $LaRhO_3$ over the 10 wt% Rh/La_2O_3 sample through XRD analysis.

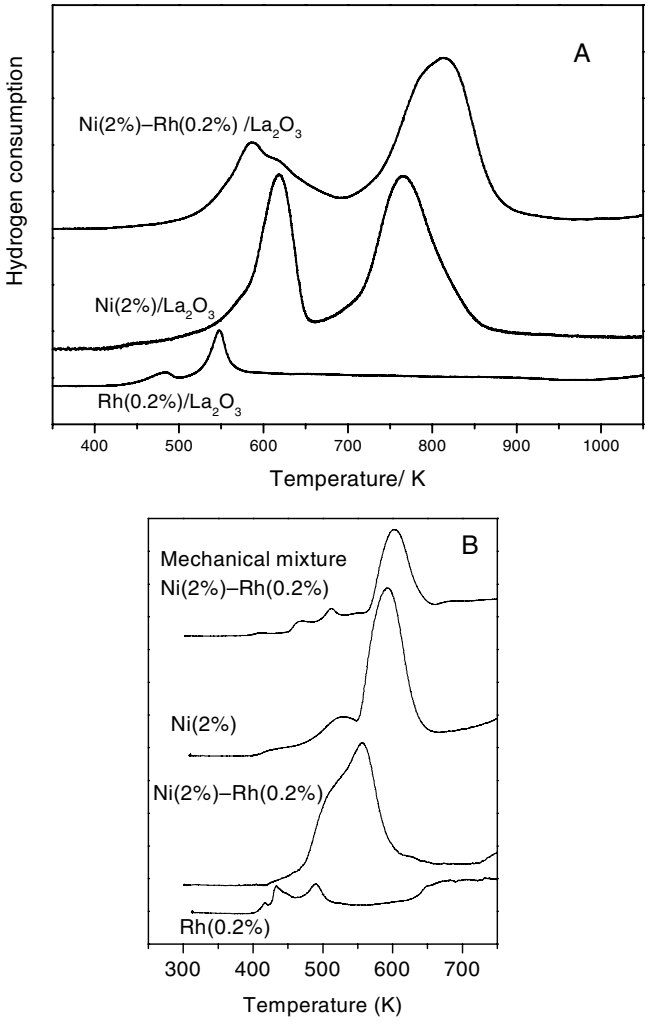

FIG. 3. TPR profiles of calcined Ni–Rh catalysts. (A) Pretreated in O_2 flow at 1123 K; (B) pretreated in O_2 at 823 K.

In the case of bimetallic Ni (2%)–Rh (0.2%) catalyst, the TPR profile is similar to the Ni (2%) solid (Fig. 3A). A small change in the reduction temperature is observed. The high-temperature peak maximum increases by 50 K, indicating a stronger interaction between nickel ions and the lanthanum support. Furthermore, the increased peak areas show that a larger number of interacting species are present in the latter case. These results led us to conclude that after treatment in oxygen at 1123 K, the solids present a strong metal–support interaction. However, even in these cases, Ni catalysts are almost totally reduced at temperatures lower than 873 K.

The TPR profiles of the Ni samples treated at 823 K (Fig. 3B) present a low-temperature peak (590 K) with higher hydrogen consumption, indicating that in these cases the proportion of well-dispersed Ni is higher than those recorded on solids treated at 1123 K.

In the case of the Rh (0.2%) catalyst, the TPR profiles are similar. The metal–support interaction is not affected by the treatment, but a higher proportion of well-dispersed Rh is observed after the low-temperature calcination. Note that the bimetallic Ni–Rh solid shows a lower reduction temperature (559 K), thus suggesting a possible interaction between the well-dispersed metals. The TPR profile of the mechanical mixture supports this analysis, because it shows separate reduction peaks similar to those observed for the monometallic ones (Fig. 3B).

XPS Characterization

For the rhodium-supported samples the Rh/La signal-intensity ratio increased from 0.067 to 0.15 with an increase in rhodium content from 0.2 to 0.6 wt% (Table 4). The Rh $3d_{5/2}$ binding energies were obtained for the calcined catalysts. The C 1s peak at 289.0 eV is attributed to carbonate carbon (14). Binding energies were referenced to C 1s = 284.6 eV, which resulted in a binding energy for La $3d_{5/2}$ = 834.6 eV in the monometallic rhodium solid. For these solids the BEs of Rh $3d_{5/2}$ were between 308.0 and 309.1 eV (Table 4). According to the literature, these

TABLE 4

Binding Energies and Surface Atomic Ratios of Ni–Rh Catalysts

Catalyst	La $3d_{5/2}$[a]	Rh $3d_{5/2}$	$(C\ 1s)_{CO_3}$[b]	$(C_{CO_3}/La)_s$	$(Ni/La)_s$	$(Rh/La)_s$
Rh (0.2%)	834.6 (3.0)	307.9 (2.3)	289.0	0.8	—	0.067
Rh (0.6%)	834.6 (3.2)	309.1 (2.1)	289.0	1.9	—	0.15
Ni (2%)–Rh (0.2%)	835.1 (3.6)	309.1 (2.6)	289.4	0.9	0.026	0.067
Ni (2%)	835.0 (3.4)	—	289.5 (2.2)	0.7	0	—

[a] FWHM is in parentheses.
[b] Contamination carbon was taken as reference at 284.6 eV.

high-energy values indicate the presence of Rh^{n+} species. Values in the range 307.6–309.6 eV for Rh^{+} compounds have been compiled by Nefedov *et al.* (15). However, other authors (16) have reported BEs for Rh^{2+} compounds within a similar range (308.4–309.3 eV).

In the Ni (2%) sample, no Ni signal was detected; however, in the bimetallic solid the Ni/La surface ratio was equal to 0.026. The Ni $2p_{1/2}$ peak was employed to calculate the surface ratio due to the overlapping of the Ni $2p_{3/2}$ and La $3d_{3/2}$ signals. In the bimetallic solid the Rh 3d peak shows a significant broadening (FWHM = 2.6 eV) and the Rh/La ratio presents the same value as in the monometallic one (Table 4).

The FWHM of Rh $3d_{5/2}$ peak reflects the particle size mainly (17, 18). The increased FWHM for small particles, where the BE is also sensitively size dependent, originates from the particle size distribution. The low-loading catalyst exhibits larger FWHM than Rh (0.6%) and the BE for Rh (0.6%) is 1 eV higher than Rh (0.2%). This indicates smaller average particle size and broader size distribution in the former solid.

Carbon Deposition

Despite the fact that all the catalysts tested did not change their activities with time on stream, TGA, DSC experiments, SEM, and Raman spectroscopy proved the presence of carbon deposits on all the solids. In the Raman spectra of all used catalysts (Fig. 4), two peaks were observed, at 1580 and 1350 cm^{-1}, in the 1200–1700 cm^{-1} region. Both peaks were due to the presence of graphitic carbon in these solids (19).

The TGA results are shown in Table 3. The weight change during the oxidation of monometallic catalysts used for 48 h (Fig. 5A) shows that there is just one peak, which starts at 950 K, for Ni (2%) and Rh (0.2%) catalysts. In the Rh (0.6%) solid a small second peak appears, at 600 K.The same peak was observed during the TGA of the calcined catalysts that showed the presence of hydroxide through XRD. Besides, the DSC experiments (Fig. 6) show that this weight loss is endothermic so it could be attributed to the $La(OH)_3$ decomposition. In the bimetallic catalyst the largest peak appears between 700 and 950 K while there is a small weight loss at higher temperature. On the other

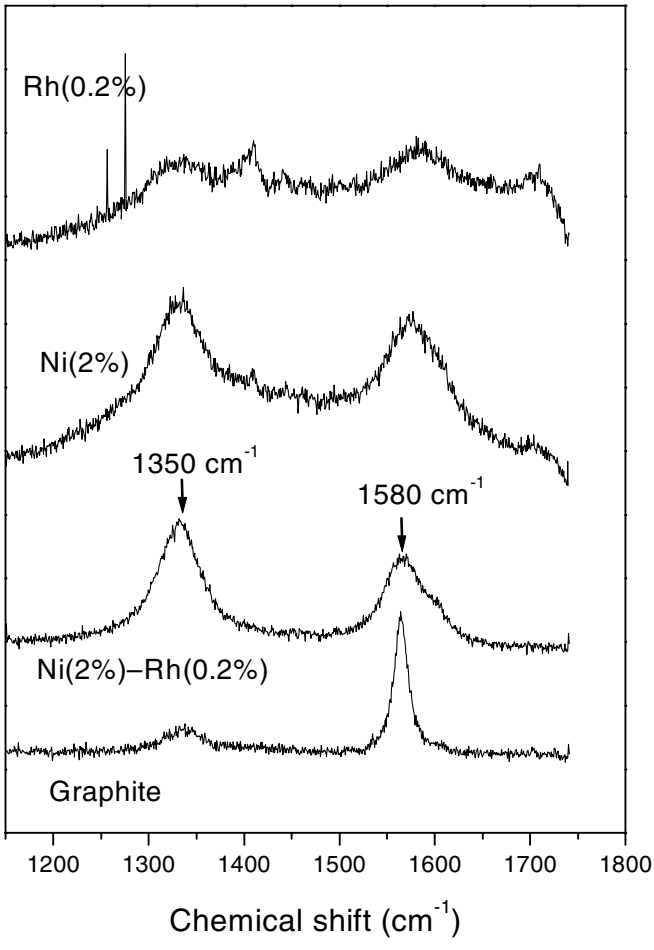

FIG. 4. Raman spectra of Ni–Rh catalysts used for 48 h in reforming reaction. Temperature range, 832–973 K; $W/F = 1.07 \times 10^{-5}$ g h ml^{-1}; 33% (v/v) CH_4; 33% CO_2; 34% He; $P = 1$ atm.

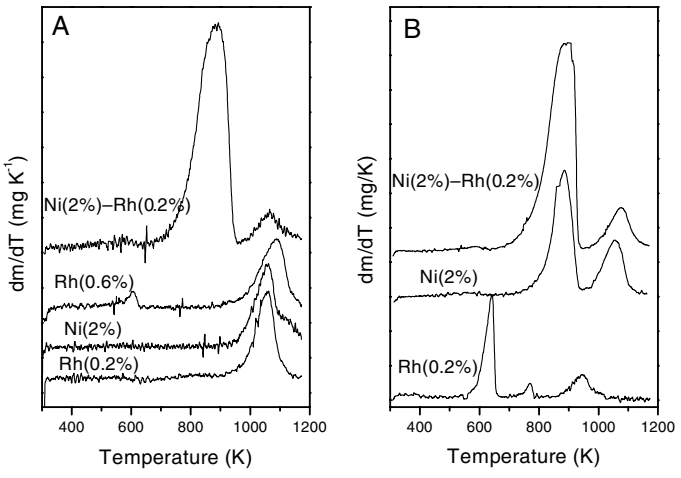

FIG. 5. DTGA profiles of used solids. (A) Used 48 h between 823 and 973 K, $W/F = 1.07 \times 10^{-5}$ g h ml^{-1}. (B) Used 100 h at 823 K, $W/F = 2.67 \times 10^{-5}$ g h ml^{-1}.

corresponds to an endothermic process (Fig. 6). Note that this peak also appears in the Rh (0.6%) used for 48 h. This peak is assigned to the dehydration of the hydroxide that could have been produced by water originating from the reverse water–gas-shift reaction. The carbon deposit on the Ni catalyst also changes with time on stream; in this case the carbonaceous species is oxidized between 800 and 900 K. The carbonaceous species on the bimetallic solid are not affected by time on stream.

After 48 h on stream with temperatures as high as 973 K, graphitic filaments were observed in the Ni–Rh solids (Fig. 7). Given the fact that the main weight loss due to an exothermic process occurs at 900 K in this catalyst, this could be assigned to the burning of filamentous carbon. This same type of carbon would appear in the Ni catalyst when used for 100 h at 823 K. By observing the micrographs the absence of the encapsulating-type carbon cannot be taken for granted but, given the catalysts stability, its nonexistence

hand, the DSC curve of this solid (Fig. 6) shows a small exothermic peak at 610 K. This could be due to the oxidation of a reactive carbonaceous deposit that is not detected by TGA. This curve also shows that the weight loss between 750 and 900 K is an exothermic process. The same TGA experiment was carried out on lanthanum oxide showing only one peak, at 1100 K, which could be due to oxycarbonate decomposition (20). This compound was detected by XRD analysis in all the solids and was also previously reported on lanthanum oxide-supported catalysts (14).

The weight-change profile for the oxidation of Rh (0.2%) catalysts used for 100 h is completely different from the one used for 48 h (Fig. 5A). Three peaks are observed in Fig. 5B; the first, at 600 K, is the most important one and

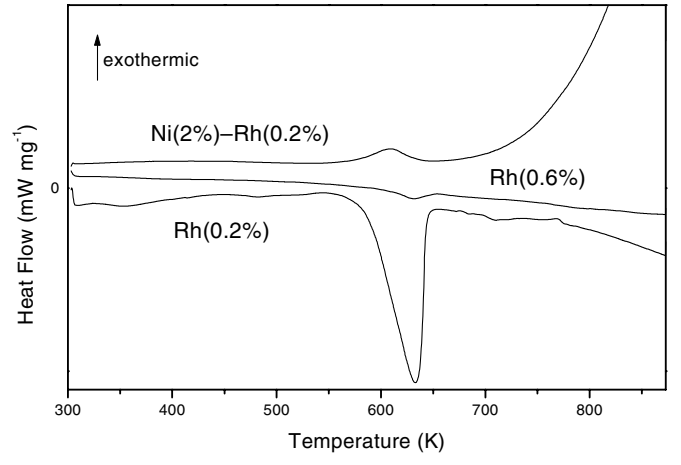

FIG. 6. DSC results of used catalysts. Ni (2%)–Rh (0.2%) and Rh (0.6%) used for 48 h between 823 and 973 K; Rh (0.2%) used for 100 h at 823 K.

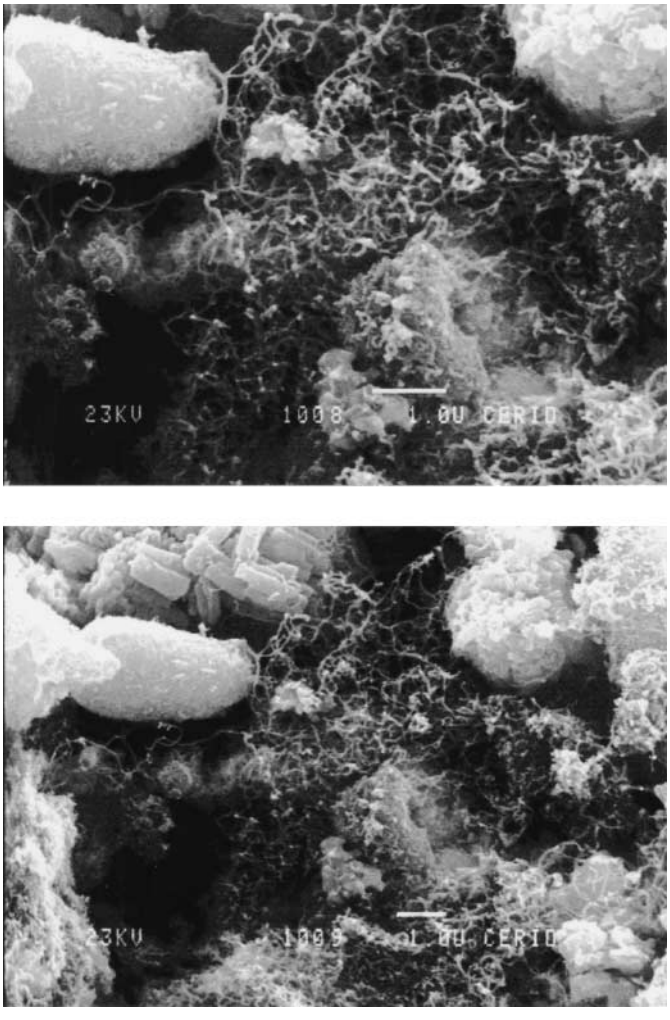

FIG. 7. SEM micrographs of Ni (2%)–Rh (0.2%) catalysts after 48 h on stream at $W/F = 1.07 \times 10^{-5}$ g h ml^{-1}; temperature range, 823–973 K.

may be inferred. In the Ni and Rh monometallic catalysts used between 823 and 973 K the presence of carbonaceous filaments was not observed by SEM. Note, however, that graphitic carbon was detected using Raman spectroscopy in all catalysts.

DISCUSSION

Catalytic Activity of Mono- and Bimetallic Ni–Rh Solids

To compare our results with the data previously reported, reaction rates and TOF values, calculated from data given by the authors, are presented in Table 2. Lercher and coworkers (6) have reported TOFs of CO_2 at 875 K for Rh catalysts supported on ZrO_2, γ-Al_2O_3, and SiO_2 (Table 2). Through deactivation studies, they concluded that the activity of their catalysts was mainly determined by the availability of Rh and was less influenced by the support. Mark and Maier (11) have calculated the CH_4 TOFs at the same temperature, employing similar supports. They found that the reaction rates per unit surface area showed no trend and concluded that the reaction is independent of the metal dispersion and the nature of the support. However, Zhang *et al.* (21) contend that the initial values of TOF obtained over their supported Rh catalysts exhibit a dependence on particle size, but this dependence might be related to metal–support interactions. In a recent paper Sigl *et al.* (9) have reported a vanadia-promoted high-loading Rh (3.8%)/SiO_2, which presents higher rates and higher TOF when compared with their 3.8 wt% Rh/SiO_2 catalyst. These conflicting results are likely to be due to differing extents of deactivation and Rh crystallite size (22).

Crisafulli *et al.* (23) reported the catalytic activity of Ni/SO_2 catalysts at 873 K (Table 2). They found results similar to ours but their solids present an average deactivation rate of 2.8% h^{-1}. Even though there are many publications concerning Ni catalysts, only a few of them reported TOF values. This could be due to the difficulties in measuring Ni dispersion (22).

Our activity data show that the catalytic behavior of the Ni–Rh-based catalysts toward the carbon dioxide reforming depends on the supported metals, and on the metal concentration in the monometallic Rh catalysts. Our Rh/La_2O_3 catalysts present the highest TOFs even at temperatures as low as 823 K (Table 2) and no deactivation was observed over the period of time assayed. For further comparison the reaction rates per gram of Rh were calculated. Note that our Rh (0.2%) catalyst shows the highest value at 823 K, the lowest temperature recorded in Table 2.

In our catalysts, addition of Rh to Ni solids caused an improvement in the reaction rates of methane and carbon dioxide measured at 823 K. On the other hand, the stability of the solids was not modified with the presence of the noble metal. However, the carbon deposition on the bimetallic sample is remarkably higher than that of both Rh and Ni monometallic catalysts. On the basis of the characterization data, these behaviors could be related to the different metal–support interactions. Using TPR a fraction of well-dispersed metal was observed while a high-temperature peak suggests the presence of a metal–support interaction. In the case of the bimetallic solid, the decrease in the TPR peak temperature could be due either to an interaction between the dispersed metals or to the presence of metallic Rh which could increase the reducibility of Ni oxide species, or to both effects. Crisafulli *et al.* (23) have studied the activity and stability for the bimetallic Ni–Ru and Ni–Pd/SiO_2 catalysts. The different catalytic performance was mainly related to the different degree of metal–metal interactions. For the Ni–Ru sample prepared with chloride precursors, they found a strong Ni–Ru interaction with a significant decrease in the hydrogen chemisorption. Garetto *et al.* (25) found that the high-temperature reduction of Pt–Ge solids strongly diminishes the hydrogen chemisorption due to the formation of alloyed bimetallic clusters. In our catalysts we observed that the simultaneous presence of both metals inhibited the hydrogen chemisorption, even though no alloyed particles were detected.

The H_2 desorption temperatures observed in our solids are higher than those reported in the literature. Studying Rh/MgO catalysts, Zhang *et al.* (21) found that both the increased desorption temperature and the decrease in the amount of H_2 adsorbed may be due to the blockage of Rh surface sites by sulfates, originating from the MgO sulfur impurities. In their case, this blockage also affects the catalytic activity of their solids. And this is not our case.

It is more likely that in our solids the higher temperatures are related to some electronic modifications of the smaller metal crystallites which interact intimately with the support. In fact, Goula *et al.* (3) have reported a significant shift to higher H_2 desorption temperatures in the NI/CaO–Al_2O_3 system which they said are due to electronic modifications occurring in the Ni crystallites ($d < 10$ nm).

Note that the XPS Ni/La intensity is measurable (Table 4) only in the Ni (2%)–Rh (0.2%) catalyst. This is symptomatic of some sort of interaction between the two metals. As a matter of fact, these two elements form alloys in all proportions (26). So, these arguments lend more weight to the hypothesis that Ni–Rh alloy formation is the cause of impaired hydrogen chemisorption in the bimetallic catalysts.

Carbon Deposition and Stability of Ni–Rh/La_2O_3 Catalysts

Catalyst deactivation and coke formation are very important factors in methane reforming with carbon dioxide. The formation of carbon deposits is a key factor when the catalyst is to be used in a membrane reactor. In general, the deactivation can be attributed to different processes, such as metal particle sintering, metal–support interaction, and carbon deposition. In our case, the catalyst activity has not been influenced by the carbon deposition after 100 h on

stream. This behavior could be related to the carbon deposition sites and/or the ability of carbon to play a role as a reaction intermediate (21).

The carbon formation at different reaction temperatures has been widely studied on supported catalysts containing either Ni at 1023 K (2, 3) or Rh at 923 (21), 875 (6), and 723 K (9). Different types of coke deposits have been reported for methane reforming on Ni catalysts, such as adsorbed atomic carbon, amorphous carbon, bulk carbide, and crystalline graphitic carbon (27). Kroll *et al.* (5) have shown that the carbon filaments do not deactivate the catalyst directly, except after a massive carbon accumulation. The carbon atoms could be dissolved in the Ni crystals and then spread through the metal, afterward precipitating between Ni and the support to form the polymeric filament. In this way, the Ni particle remains on the filament tip, thus explaining the stability of catalysts containing Ni, despite the large amount of carbonaceous deposit (28). The deactivating coke was identified as a polymorphic form of graphite which develops as veils around the Ni particles, suppressing the access of reactants to the metal surface.

A very stable Ni/ZrO_2 catalyst was reported by Wei *et al.* (29). They assigned the higher stability to the low carbon deposition, which in turn is connected to an enhanced migration of the active oxygen atoms to the active sites. This is due to higher concentration of oxygen defects on basic sites for CO_2 activation near the nickel-support perimeter derived from the ultrafine hydroxide precursor.

In Ni/La_2O_3 catalysts, an unusual catalytic stability was reported by Slagtern *et al.* (2). This effect would be related to the catalyst morphology. The tight coating of the nickel particles by layers of lanthanum carbonate could hinder the formation of deactivating coke, possibly by limiting the carbon migration through the nickel particles and its recombination as an encapsulating veil around the particle. Taking into account the high C 1s BE obtained for our samples, it can be concluded that the C 1s peak at 289.2 eV is due to the presence of surface carbonate species in the oxides, in agreement with the bulk XRD results.

There is no general agreement about the role played by the support in the case of rhodium (6, 11, 13). In our case, the strong interaction between Rh and La oxide is probably responsible for the high stability of these solids. Does this interaction appear because at the high temperatures of the reforming reaction part of the Rh is reoxidized by CO_2? Is the rhodium oxide the one interacting with the support (13)? Even though $LaRhO_3$ formation has not been detected in our catalysts, our TPR and XPS data suggest that the stability of Rh (0.2%) is due to the strong metal–support interaction.

Verykios and co-workers (21) have reported the formation of different types of active carbon species on Rh-supported catalysts. One of them was oxidized at low temperatures (373 K) and was assigned to a carbidic form. This species was not detected in our Ni–Rh catalysts. A second graphitic type was reported which was oxidized in the 453- to 775-K range. The high-temperature peak (1100 K) observed in our TGA experiments might be the contribution of oxycarbonate decomposition from the support and the combustion of a very stable carbon species. The presence of graphitic carbon was detected in all the used catalysts by Raman spectroscopy.

Zhang *et al.* (21) have reported that the carbon deposit formed during reaction could be transformed in less active types with increasing time on stream (ca. 10 min to 2 h). In our Ni monometallic catalysts, the carbon deposition after 100 h on stream led to a more reactive species that burnt out at 900 K. These species could be the graphitic filaments observed by SEM (Fig. 7). The presence of this nondeactivating coke explains the stability of our catalysts containing Ni, despite the large amount of carbonaceous deposits (28). In the case of our bimetallic catalyst, this could be the most abundant species. The increase in surface area found for Ni and Ni–Rh solids is consistent with this assignment.

CONCLUSIONS

In our Ni–Rh catalysts, the formation of carbon species does not affect the activity after 100 h on stream at 823 K (Fig. 2).

The Rh catalysts are stable and present the lowest carbon deposition at 823 K. Compared with other supported Rh catalysts reported in the literature, our Rh (0.2%) formulation is by far the most active one on a per-gram-of-rhodium basis (Table 2). A significant metal–support interaction, hinted at by TPR and XPS, seems to be responsible for the high activity and stability of these catalysts. Thus, this solid is the prime candidate for use in membrane reactors when the reaction temperature must be kept below 873 K and where the absence of carbon deposition is a basic requisite.

ACKNOWLEDGMENTS

The authors wish to acknowledge the financial support received from UNL, CONICET, and ANPCyT. Thanks are given to the Japan International Cooperation Agency (JICA) for the donation of the major instruments, to Elsa Grimaldi for the editing of the English manuscript, to Fabricio Charles and Carolina Mosimann for their technical assistance, and to Prof. María Alicia Ulla for her helpful discussions.

REFERENCES

1. Prabhu, A., and Oyama, T., *J. Membrane Sci.* **176**, 233 (2000).
2. Slagtern, A., Schuurman, Y., Leclercg, L., Verykios, X., and Mirodatos, C., *J. Catal.* **172**, 118 (1997).
3. Goula, M., Lemonidou, A., and Efstathiou, A., *J. Catal.* **161**, 626 (1996).
4. Chang, J., Park, S., Yoo, J., and Park, J., *J. Catal.* **195**, 1 (2000).
5. Kroll, V., Swaam, H., and Mirodatos, C., *J. Catal.* **161**, 409 (1996).
6. Bitter, J. H., Seshan, K., and Lercher, J. A., *J. Catal.* **176**, 93 (1998).

7. Bradford, M., and Vannice, A., *J. Catal*. **183**, 69 (1999).
8. Bitter, J. H., Seshan, K., and Lercher, J. A., *J. Catal.* **183**, 336 (1999).
9. Sigl, M., Bradford, M., Knözinger, H., and Vannice, M., *Top. Catal.* **8**, 211 (1999).
10. Kikuchi, E., and Chen, Y., *Stud. Surf. Sci. Catal*. **107**, 547 (1997).
11. Mark, M., and Maier, W., *J. Catal.* **164**, 122 (1996).
12. Brown, R., Cooper, M., and Whan, D., *Appl. Catal.* **3**, 177 (1982).
13. Wang, H., and Ruckeinstein, E., *Appl. Catal. A* **204**, 143 (2000).
14. Milt, V., Spretz, R., Ulla, M., Lombardo, E., and García Fierro, J., *Catal. Lett.* **42**, 57 (1996).
15. Nefedov, V. I., Shubochikina, E. F., Kolomnikov, I. S., Baranovskii, I. B., Golubnichaya, V. P., Chubochkin, L. K., Porai-Koshits, M. A., and Vol'pin, M. E., *Russ. J. Inorg. Chem.* **18**, 444 (1973).
16. Gysling, H., Monnier, J., and Apai, G., *J. Catal*. **103**, 407 (1987).
17. Cheung, T. T., *Surf. Sci.* **140**, 151 (1984).
18. Zafeirotos, S., Nehasil, V., and Ladas, S., *Surf. Sci.* **433–435**, 612 (1999).
19. Tuinstra, F., and Koenig, J., *J.Chem.Phys*. **53**, 1126 (1970).
20. Turcotte, R. P., Sawyer, J. O., and Eyring, L., *Inorganic Chem*. **8**(2), 238 (1969).
21. Zhang, Z., Tsipouriari, V., Efstathiou, A., and Verykios, X., *J. Catal.* **158**, 51 (1996).
22. Bradford, M., and Vannice, A., *Catal. Rev.–Sci. Eng*. **41**(1), 1 (1999).
23. Crisafulli, C., Sciré, S., Maggiore, R., Minicò, S., and Galvagno, S., *Catal. Lett.* **59**, 21 (1999).
24. Bartholomew, C. H., *Catal. Lett.* **17**, 27 (1990).
25. Garetto, T., Borgna, A., and Apesteguía, C., *Stud. Surf. Sci. Catal*. **101**, 1155 (1996).
26. Moffett, W., "The Handbook of Binary Phase Diagrams," Vol. 4. General Electric Co., 1978.
27. Kim, J., Suh, D., Park, T., and Kim, K., *Appl. Catal. A* **197**, 191 (2000).
28. Tsang, S., Claridge, J., and Green, M., *Catal. Today* **23**, 3 (1995).
29. Wei, J., Xu, B., Cheng, Z., Li, J., and Zhu, Q., *Stud. Surf. Sci. Catal.* **130**, 3687 (2000).